GEOPHYSICS, VOL. 71, NO. 6 (NOVEMBER-DECEMBER 2006); P. R79–R90, 13 FIGS.
10.1190/1.2336347

A novel approach to the model appraisal and resolution analysis of regularized geophysical inversion

Michael S. Zhdanov[1] and Ekaterina Tolstaya[1]

ABSTRACT

The existing techniques for appraisal of geophysical inverse images are based on calculating the model resolution and the model covariance matrices. In some applications, however, it becomes desirable to evaluate the upper bounds of the variations in the solution of the inverse problem. It is possible to use the Cauchy inequality for the regularized least-squares inversion to quantify the ability of an experiment to discriminate between two similar models in the presence of noise in the data. We present a new method for resolution analysis based on evaluating the spatial distribution of the upper bounds of the model variations and introduce a new characteristic of geophysical inversion, resolution density, as an inverse of these upper bounds. We derive an efficient numerical technique to compute the resolution density based on the spectral Lanczos decomposition method (SLDM). The methodology was tested on 3D synthetic linear and nonlinear electromagnetic (EM) data inversions, and also to interpret the helicopter-borne EM data collected by INCO Exploration in the Voisey's Bay area of Canada.

INTRODUCTION

The results of geophysical data interpretation are usually presented in the form of a corresponding model of the earth's formations in the area of investigation. We determine this model by solving the inverse problem for geophysical data, which are contaminated by noise and are acquired at a limited number of observation points. Because of the ill-posed nature of inverse geophysical problems, the solutions are ambiguous and unstable. There are always many solutions that will fit the observed noisy data practically with the same data misfit. The variations of the inverse model parameters may be unreasonably large if we do not use regularization (Tikhonov and Arsenin, 1977). There are still significant uncertainties, however, even with the application of regularization to the inverse-problem solution. The question arises, What are the maximum possible variations of the model parameters that would preserve the variation of the predicted data within the level of the noise in the observations? In other words, what is the practical resolution of the regularized inversion?

This is one of the most important problems of exploration geophysics. This problem arises in the initial stage of a geophysical investigation when we design the geophysical survey. The same problem appears at the final stage when we examine the results of the interpretation of the observed geophysical data. Actually, the question about sensitivity and resolution of the given geophysical method is usually the first one asked by geologists working with geophysical data.

The sensitivity of the geophysical method is determined as the ratio of the variation of the data to the variation of the model parameters. The sensitivity can be found by direct modeling of the theoretical response for the given model perturbation, or by using a reciprocity principle (Rodi, 1976; McGillivray and Oldenburg, 1990; McGillivray et al., 1994; Spies and Habashy, 1995; Zhdanov, 2002).

The word *resolution* was introduced into geophysical inversion by Backus and Gilbert in their classic 1967 and 1968 papers about analysis of the general resolution power of the corresponding geophysical method. In this paper, we are interested, instead, in the resolution study of a specific, regularized inversion of given geophysical data. In this sense, our approach provides the model appraisal of the regularized inversion. However, for this analysis, we use a mathematical technique, which is quite different from the ones discussed in previous publications (see, for example, Ramirez et al., 1995; Alumbaugh and Newman, 2000).

The existing techniques for appraisal of geophysical inverse images are based primarily on calculating of the data and model resolution and covariance matrices (Tarantola, 1987; Menke, 1989; Alumbaugh and Newman, 2000). These matrices make possible the a posteriori appraisal of the quality of the geophysical inversion by displaying a distribution of the variances of the model parameter $\mathbf{m}$, which describes a standard deviation of the model parameters from

Manuscript received by the Editor August 31, 2004; revised manuscript received April 9, 2006; published online September 26, 2006.
[1]University of Utah, Department of Geology and Geophysics, Salt Lake City, Utah. E-mail: mzhdanov@mines.utah.edu.

the inversion result. In geophysical applications, however, it may be useful to also estimate the upper bounds of the variations in the solution of the inverse problem for the given errors in the observed data. These upper bounds of the model variations confine the actual resolution of the geophysical inversion. In this paper, we introduce a new characteristic of geophysical inversion, *resolution density*, which is determined as the inverse of the upper bounds of the model parameter variations, and develop a method for solving this problem.

There have been previous examples of inversion procedures for generating the bounds on variables [see, for example, Parker (1975) on the theory of ideal bodies for gravity interpretation, Sabatier (1977a, 1977b, 1977c) on linear inverse problems with constraints, Oldenburg (1983) on funnel functions, and Stark et al. (1986) and Stark and Parker (1987) on tau-p inversions for seismic data interpretation]. However, the previous publications were focused mostly on constructing all kinds of extreme solutions for a specific geophysical problem, e.g., on finding the smallest envelope containing all velocity profiles consistent with the seismic data (Stark et al., 1986) or looking for an ideal body as one whose supremum is the smallest of all suprema of all solutions of the gravity inverse problem (Parker, 1975).

Here, we consider the problem of evaluating the spatial distribution of the upper bounds of the model parameter variations for the given inversion result. We introduce a novel approach to solving this problem using the Cauchy inequality for the regularized least-squares inversion. In the framework of this approach, we develop a method of resolution analysis for both the linear and nonlinear inverse problems. We also develop a numerical method of resolution-density computation based on the spectral Lanzcos decomposition method (SLDM), which provides an efficient way of solving this problem for different values of the regularization parameter α (Zhdanov, 2002).

The method is illustrated by the resolution study of 3D electromagnetic (EM) inversions of airborne and magnetotelluric (MT) data. The case history includes interpretation of the helicopter-borne EM data collected by INCO Exploration in the Voisey's Bay area of Canada. We believe this new technique provides a useful tool for the analysis of the robustness of geophysical inversion.

RESOLUTION OF GEOPHYSICAL INVERSION

A strict mathematical definition of the resolution of a geophysical method was introduced in Dmitriev et al. (1990); see also Zhdanov (2002, p. 31). According to this definition, the measure of the resolution R of the given geophysical method is determined as the inverse of the norm of the inverse operator:

$$R = \frac{1}{\|A^{-1}\|}, \tag{1}$$

where A is a linear forward-modeling operator for the given geophysical problem. This definition comes from the equality

$$\Delta_{\max} = \|A^{-1}\|\delta = \frac{\delta}{R}, \tag{2}$$

where $\Delta_{\max}$ is the maximum possible error in the solution of the inverse problem for the given level of errors in the observed data δ. Based on the last equations, one can say that two models, $\mathbf{m}_1$ and $\mathbf{m}_2$, can be resolved if the following condition is satisfied:

$$\|\mathbf{m}_1 - \mathbf{m}_2\| \geq \Delta_{\max} = \frac{\delta}{R}.$$

The smaller the norm of the inverse operator, the larger the resolution R and the closer to each other are the models that can be resolved. If the inverse operator A^{-1} is not bounded, i.e., its norm goes to infinity, the resolution goes to zero, $R = 0$, and the maximum possible variations in the determination of $\mathbf{m}$ are infinitely large. This situation appears in the case of ill-posed problems (Zhdanov, 2002). Note, however, that the aforementioned definition provides a global estimate of the resolution in the sense that we can estimate only a norm of the difference between two models that must be resolved. At the same time, it would be very important to be able to compute a local estimate of the resolution (resolution density), which would deliver a distribution of the upper bounds of the model parameter variations in the regularized solution of the inverse problem for the given level of the errors in the observed data.

Many papers analyze the effect of errors on the geophysical inverse problem solution (e.g., Sabatier, 1977a, b, c; Stark et al., 1986; Stark and Parker, 1987; Menke, 1989). Generally speaking, there are two major points of view in addressing this problem:

1) The algebraic (deterministic) point of view [dating back to Lanczos (1961), Marquardt (1963, 1970), Backus and Gilbert (1967, 1968), Backus (1970a, b, c), and Tikhonov and Arsenin (1977)].
2) The stochastic (probabilistic) point of view [formulated in the pioneering papers of Foster (1961), Franklin (1970), Jackson (1972), Tarantola and Valette (1982), and Tarantola (1987)].

The stochastic point of view is widely used in geophysical literature because it is closely associated with the statistical nature of noise in geophysical data (see Sambridge and Mosegaard, 2002). We would like to recall, however, Sabatier's remark (1977a, p. 125), "if one trusts a certain statistical interpretation of errors, and ergodicity, the solutions can be classed according to one's degree of confidence." At the same time, it has been demonstrated in many publications [e.g., the classic work by Sabatier (1977a) that both points of view result in similar computational algorithms].

We analyze the solution of the geophysical inverse problem based on Tikhonov regularization, which corresponds to the algebraic (deterministic) point of view (Tikhonov and Arsenin, 1977).

RESOLUTION DENSITY

Let us consider a linear matrix equation:

$$\mathbf{d} = \mathbf{A}\mathbf{m}. \tag{3}$$

Here, $\mathbf{m}$ is the vector of the model parameters of order N_m, $\mathbf{d}$ is the vector of the observed geophysical data of order N_d, and the matrix $\mathbf{A}$ is the $N_d \times N_m$ matrix of the linear forward-modeling operator.

In the framework of Tikhonov regularization theory, the regularized solution of this inverse problem can be based on the parametric functional minimization:

$$\begin{aligned} P^{\alpha}(\mathbf{m},\mathbf{d}) &= (\mathbf{W}_d\mathbf{A}\mathbf{m} - \mathbf{W}_d\mathbf{d})^*(\mathbf{W}_d\mathbf{A}\mathbf{m} - \mathbf{W}_d\mathbf{d}) \\ &\quad + \alpha(\mathbf{W}_m\mathbf{m} - \mathbf{W}_m\mathbf{m}_{\text{apr}})^*(\mathbf{W}_m\mathbf{m} - \mathbf{W}_m\mathbf{m}_{\text{apr}}) \\ &= \min, \end{aligned} \tag{4}$$

where $\mathbf{W}_d$ and $\mathbf{W}_m$ are some weighting matrices of the data and model parameters; $\mathbf{m}_{apr}$ is some a priori model; $*$ denotes the complex conjugate transpose matrix; and α is a regularization parameter. The detailed description of the optimal weighting matrices selection is given in Zhdanov (2002).

A solution of the general least-squares problem of equation 4 is given by the following equations (Tikhonov and Arsenin, 1977):

$$\mathbf{m}_\alpha = (\mathbf{A}^*\mathbf{W}_d^2\mathbf{A} + \alpha\mathbf{W}_m^2)^{-1}(\mathbf{A}^*\mathbf{W}_d^2\mathbf{d} + \alpha\mathbf{W}_m^2\mathbf{m}_{apr}). \quad (5)$$

Let us apply the variational operator δ to both sides of equation 5:

$$\delta\mathbf{m}_\alpha = (\mathbf{A}^*\mathbf{W}_d^2\mathbf{A} + \alpha\mathbf{W}_m^2)^{-1}\mathbf{A}^*\mathbf{W}_d^2\delta\mathbf{d}. \quad (6)$$

We shall call the matrix

$$\mathbf{R}_\alpha = (\mathbf{A}^*\mathbf{W}_d^2\mathbf{A} + \alpha\mathbf{W}_m^2)^{-1}\mathbf{A}^*\mathbf{W}_d^2 \quad (7)$$

a *regularized inverse matrix*. It is measured in the following units:

$$[\text{units of } \mathbf{R}_\alpha] = \frac{[\text{units of } \mathbf{m}]}{[\text{units of } \mathbf{d}]}.$$

The spatial variations of the resolution of the geophysical inversion can be found by individually analyzing the columns of matrix $\mathbf{R}_\alpha$. Indeed, equation 6 in scalar notation can be written as

$$\delta m_i = \sum_{j=1}^{N_d} R_{\alpha ij}\delta d_j,$$

where $R_{\alpha ij}$ are the scalar components of $\mathbf{R}_\alpha$, and δm_i and δd_j are the components of vectors $\delta\mathbf{m}_\alpha$ and $\delta\mathbf{d}$, respectively.

From the Cauchy inequality, we have

$$|\delta m_i|^2 \le \sum_{j=1}^{N_d}|R_{\alpha ij}|^2\sum_{j=1}^{N_d}|\delta d_j|^2 = \varepsilon^2/\mathcal{R}_i^2, \quad (8)$$

where

$$\mathcal{R}_i = \|\mathbf{d}\|^{-1}\left[\sum_{j=1}^{N_d}|R_{\alpha ij}|^2\right]^{-1/2} \quad (9)$$

and

$$\varepsilon = \|\delta\mathbf{d}\|/\|\mathbf{d}\|$$

is a norm of the relative errors in the data. Note that the term $\sum_{j=1}^{N_d}|R_{\alpha ij}|^2$ represents a sum of the squares of the scalar components located in the ith column of $\mathbf{R}_\alpha$. We can introduce a diagonal matrix $\mathcal{R}$ formed by the elements $\mathcal{R}_i$, $i = 1,2,\ldots,N_m$. According to equation 9, this matrix is related to the regularized inverse matrix $\mathbf{R}_\alpha$ by the equation

$$\mathcal{R} = \|\mathbf{d}\|^{-1}[\mathbf{diag}(\mathbf{R}_\alpha\mathbf{R}_\alpha^*)]^{-1/2}. \quad (10)$$

We will call the diagonal matrix $\mathcal{R}$ a resolution density matrix.

Note that the resolution density matrix is computed based on the regularized inverse matrix $\mathbf{R}_\alpha$. The last matrix, according to equation 7, is not a function of the data but of the operator of the forward problem, the data and model parameters weights $\mathbf{W}_d^2$ and $\mathbf{W}_m^2$ used in the inversion, and the regularization parameter α. As a result, the resolution density depends on the physics of the method used to collect data, source-receiver configuration, data components, coverage, etc. Therefore, similar to data and model resolution and covariance matrices (Menke, 1989), this matrix is affected by the geophysical methods under consideration and data acquisition parameters only.

Now we can determine the upper bounds of the variations in the solution of the inverse problem for the given relative errors in the observed data, equal to ε:

$$\Delta_{i\,\max} = \sup_{\|\delta\mathbf{d}\|=\delta}|\delta m_i| = \varepsilon\|\mathbf{d}\|\left[\sum_{j=1}^{N_d}|R_{\alpha ij}|^2\right]^{1/2} = \varepsilon/\mathcal{R}_i. \quad (11)$$

Based on the last equations, we can determine the resolution density of the inverse problem solution. Two models, $\mathbf{m}^{(1)}$ and $\mathbf{m}^{(2)}$, in the vicinity of the point $\mathbf{m}_0$ can be resolved if the following condition is satisfied:

$$|m_i^{(1)} - m_i^{(2)}| \ge \Delta_{i\,\max} = \frac{\varepsilon}{\mathcal{R}_i}. \quad (12)$$

Thus, the upper bounds of the variations in the solution of the inverse problem are proportional to the relative errors in the data ε. Note that the noise in the data affects the upper bounds of the model variations only; it does not affect the resolution density matrix introduced above. At the same time, equation 12 provides an appraisal of the inverse problem solution by taking into account the errors (noise) in the data, the physics of the method used to collect the data, and the data acquisition parameters. The value $\mathcal{R}_i$ is also related to the weights of the data and model and the regularization parameter α used in the inversion algorithm.

The value $\mathcal{R}_i$ is the measure of the resolution density for the given inverse problem solution. It is measured in the following units:

$$\text{Resolution density: } [\text{units of } \mathcal{R}_i] = \frac{1}{[\text{units of } \mathbf{m}]}. \quad (13)$$

The larger the resolution density $\mathcal{R}_i$, the closer to each other are the models that can be resolved. The low-resolution density $\mathcal{R}_i$ corresponds to the area where even very different models cannot be resolved. Note that both the maximum possible variations $\Delta_{i\,\max}$ and the resolution density $\mathcal{R}_i$ depend on the cell number i. Thus, they describe the spatial distribution of the variations in the inverse-problem solution and of the resolution. By knowing the distribution of the resolution density in the area of inversion, we can identify the parts of the inverse model that are well resolved and the parts that are poorly resolved. Therefore, both the upper bound of the model variations and the resolution density provide effective tools for a posteriori appraisal of the regularized inversion. It is important to notice that our model appraisal and resolution analysis method takes into account the errors (noise) in the data, the physics of the method used to collect the data, the data acquisition parameters, and the inversion algorithm.

Numerical calculation of the resolution density is a very challenging computational problem. In Appendix A, we present an efficient algorithm for determining this parameter based on the SLDM (Lanczos, 1961; Druskin and Knizhnerman, 1994; Golub and Van Loan, 1996; Druskin et al., 1999; Zhdanov, 2002). The advantage of the SLDM method is that it allows us to compute the resolution density for all possible values of the regularization parameter α (Zhdanov, 2002).

RESOLUTION OF THE NONLINEAR INVERSE PROBLEM

We presented a method for the resolution analysis of the linear inverse problem. A similar technique can be introduced for nonlinear inverse-problem solution as well. Consider a nonlinear matrix equation

$$\mathbf{d} = \mathbf{B}(\mathbf{m}), \tag{14}$$

where $\mathbf{B}$ is the nonlinear forward operator. Let us assume that $\mathbf{m}_0$ is a solution of the nonlinear inverse problem obtained by some inversion method. Let us perturb equation 14 in the vicinity of point $\mathbf{m}_0$,

$$\delta\mathbf{d} = \mathbf{F}_0\delta\mathbf{m}, \tag{15}$$

where $\delta\mathbf{m}$ and $\delta\mathbf{d}$ are the perturbations of the model parameters and the data, respectively, and $\mathbf{F}_0$ is the Fréchet derivative matrix at $\mathbf{m}_0$. Our goal is to find out how the errors in the observed data $\delta\mathbf{d}$ will be transformed in the errors of the inverse-problem solution $\delta\mathbf{m}$. To solve this problem, we consider the regularized solution of equation 15, which can be expressed in the form (Zhdanov, 2002)

$$\delta\mathbf{m}_\alpha = (\mathbf{F}_0^*\mathbf{W}_d^2\mathbf{F}_0 + \alpha\mathbf{W}_m^2)^{-1}\mathbf{F}_0^*\mathbf{W}_d^2\delta\mathbf{d}. \tag{16}$$

We call matrix $\mathbf{R}_\alpha(\mathbf{m}_0)$,

$$\mathbf{R}_\alpha(\mathbf{m}_0) = (\mathbf{F}_0^*\mathbf{W}_d^2\mathbf{F}_0 + \alpha\mathbf{W}_m^2)^{-1}\mathbf{F}_0^*\mathbf{W}_d^2, \tag{17}$$

a regularized inverse matrix of the nonlinear inverse problem at a point $\mathbf{m}_0$.

Similar to the linear case, one can analyze, based on $\mathbf{R}_\alpha(\mathbf{m}_0)$, the maximum possible errors in model parameter distribution for the given level of errors in the observed data:

$$|\delta m_i|^2 \le \frac{\varepsilon^2}{\mathcal{R}_{0i}^2} \tag{18}$$

where

$$\mathcal{R}_{0i}^2 = \left(\|\mathbf{d}\|^2\sum_{j=1}^{N_d}|R_{\alpha ij}(\mathbf{m}_0)|^2\right)^{-1} \tag{19}$$

and ε is a level of relative errors in the observed data:

$$\varepsilon = \|\delta\mathbf{d}\|/\|\mathbf{d}\|.$$

The value $\mathcal{R}_{0i}$ is the measure of the resolution density for the given nonlinear inverse-problem solution $\mathbf{m}_0$.

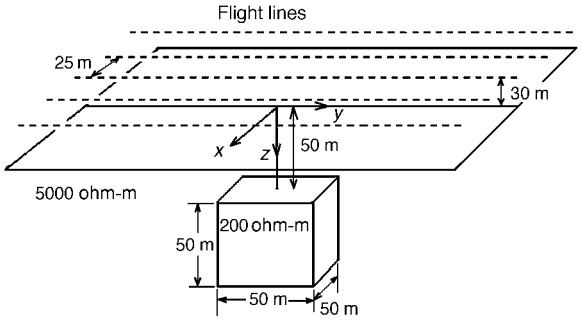

Figure 1. Schematic view of a conductive cubic model located within a resistive half-space and of a model HEM survey comprising five flight lines.

Inequality 18 allows us to determine the maximum possible errors in the solution of the nonlinear inverse problem for the given errors in the observed data, using the equation similar to expression 11.

The numerical technique for finding $\mathcal{R}_{0i}$ is similar to one developed for a linear inverse problem in Appendix A. The only difference is that we must substitute the linear forward-modeling operator by the Fréchet derivative in the corresponding equations of resolution analysis.

RESOLUTION STUDY OF THE LINEARIZED INVERSION OF A 3D SYNTHETIC HELICOPTER-BORNE EM SURVEY

In this section, we illustrate the developed method of the resolution analysis for the linearized airborne EM data inversion. Helicopter-borne EM (HEM) surveys are widely used in mineral exploration. The main difficulties in the modeling and interpretation of HEM data are related to the fact that for any new observation point, one must solve the forward problem anew for the corresponding position of the moving transmitter. In this situation, even forward modeling of HEM data over inhomogeneous structures requires an enormous number of computations. That is why, until recently, the interpretation of HEM data was restricted to simple 1D inversion. Zhdanov and Tartaras (2002) developed a new approach to the modeling and inversion of multisource array EM data based on the so-called localized quasi-linear (LQL) approximation. In the framework of this approach, forward modeling and inversion of multisource data can be calculated at the same time for all different positions of the transmitters. The LQL approximation also reduces the HEM data inversion to the solution of the linear inverse problem, which makes it possible to implement the linear resolution analysis developed in the previous sections of the paper.

In the original paper by Zhdanov and Tartaras (2002), the linear EM inverse problem was solved using the conjugate gradient (CG) method. Zhdanov and Chernyavskiy (2004) introduced a new technique for fast LQL inversion that employs the SLDM method (Druskin and Knizhnerman, 1994; Golub and Van Loan, 1996; Druskin et al., 1999; Zhdanov, 2002). This technique helps to accelerate HEM data inversion and provides a stable image of the geoelectrical target. We use a similar technique for the resolution analysis as well (see Appendix A).

First, we consider a synthetic example of the resolution analysis of the HEM data inversion. We apply the integral equation software SYSEM (Xiong, 1992) to simulate such a survey over a relatively conductive (200 ohm-m) cubic body located in a resistive (5000 ohm-m) half-space. Figure 1 depicts a 3D view of the model. Five lines were flown over the target at an altitude of 30 m and at a distance of 25 m apart. A schematic 3D view of the survey is shown in Figure 1.

The moving transmitter-receiver system was a pair of vertical magnetic dipoles (simulating a horizontal coplanar coil pair) and a pair of horizontal magnetic dipoles (simulating a vertical coaxial coil pair) with 8 m of horizontal separation. The *yy* (coaxial) and *zz* (coplanar) components of the anomalous magnetic field were measured every 15 m along the lines (50 observation points in each line). A 7.2-kHz frequency was used.

We added 1% random noise to the anomalous magnetic field and then inverted it using the SLDM method. The area of inversion, centered around the body, was 150 m × 150 m × 150 m and was divided into 12 × 12 × 12 cells.

Figure 2 shows the vertical cross sections (along the x-axis) of the 3D model obtained as a result of the regularized inversion with the minimum norm stabilizer (Zhdanov and Chernyavskiy, 2004). We should note that the inversion provides a correct position of the target but underestimates the true conductivity of the body. Indeed, the recovered resistivity for the body is about 1000 ohm-m, while the true resistivity of the body is 200 ohm-m. This result comes without any surprise because it is well known that the linearized smooth inversion tends to underestimate the true physical parameters of the target (see, for example, Zhdanov, 2002, p. 46–49). To recover the correct conductivity, one should use the nonlinear inversion with the focusing stabilizer, which will be outlined in the next numerical example of the MT data inversion. This is, however, a very challenging problem in the case of HEM data collected with the moving transmitter-receiver pairs because any new position of the transmitter requires solving a different forward-modeling problem. The full 3D nonlinear inversion for the multitransmitter airborne data is still impractical because of the huge computational time required in this case. At the same time, a linearized approach represents an effective solution of 3D inverse problem for the multitransmitter EM data, which can be widely used in practical interpretation of HEM data. We should also note that the limitations of the fast-forward mapping operators in inverse-problem solution are addressed in many publications, including Zhdanov and Tartaras (2002) and Zhdanov and Chernyavskiy (2004). The errors in these approximations affect the uncertainty analysis in the same way that they affect the inversion result itself. In this situation, it is especially important to evaluate how robust the linearized inversion is with respect to the noise in the data. The new method of model appraisal and resolution analysis provides the corresponding mathematical technique for solving this problem.

Using the general resolution theory outlined above, we can find the resolution density $\mathcal{R}_i^{\Delta\sigma}$ and the upper bounds of the conductivity variations, according to

$$\delta\Delta\sigma_i = \frac{\varepsilon}{\mathcal{R}_i^{\Delta\sigma}}.$$

The vertical cross sections of the upper bounds of the conductivity variations $\delta\Delta\sigma_i$ for the cubic model inversion are shown in Figure 3, while Figure 4 presents the $\mathcal{R}_i^{\Delta\sigma}$ distribution. We have assumed in these calculations that the relative error in the observed data is $\varepsilon = 1\%$. We can see in Figure 3 that the estimated variations in the HEM data inversion in the area of the cubic body are within 0.00001 S/m, while the estimated inverted conductivity of the body is about 0.001 S/m. Thus, the variations do not exceed 1%, which corresponds well to 1% level of noise in the data. This fact demon-

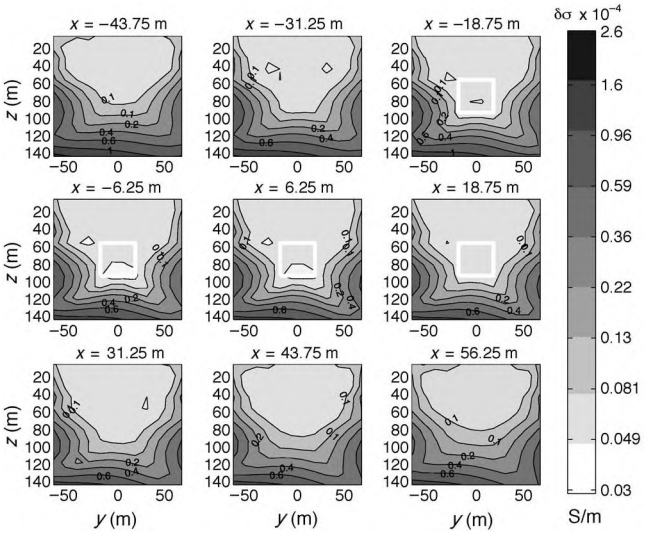

Figure 3. The vertical cross sections of the upper bounds of the conductivity variations $\delta\Delta\sigma_i(\mathbf{r})$ computed for the cubic model HEM data inversion under the assumption that the relative error in the observed data is $\varepsilon = 1\%$. The white outlines show the true contour of the conductive body.

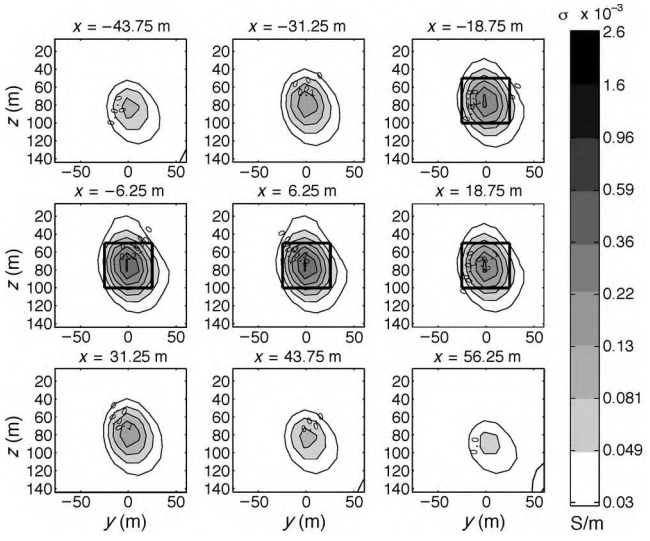

Figure 2. The vertical cross sections (along the x-axis) of the 3D model obtained as a result of regularized inversion for the synthetic observed HEM data for a conductive cubic model. The black outlines show the true contour of the conductive body.

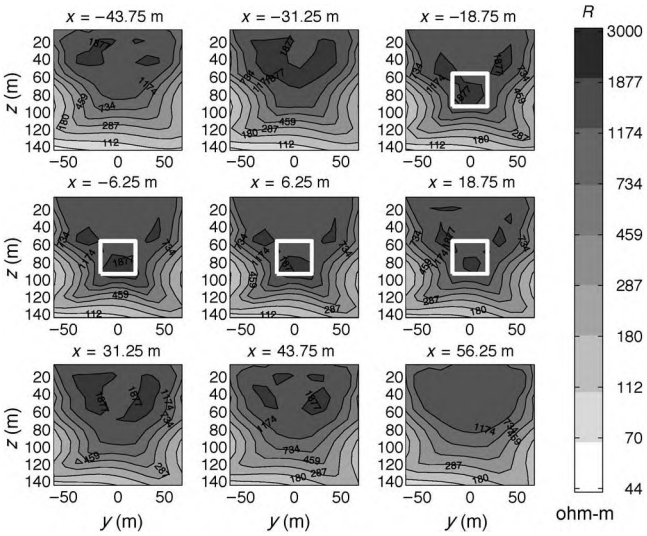

Figure 4. The vertical cross sections of the resolution density $\mathcal{R}_i^{\Delta\sigma}$ distribution for the cubic model HEM data inversion. The white outlines show the true contour of the conductive body.

strates that our inversion algorithm does not amplify the noise in the data

Based on this analysis, we can conclude that the LQL inversion outlined above is a very robust method. It provides a stable geometric image of the target while underestimating the true conductivity. We should note, however, that the detailed analysis of Figure 3 shows that this robust solution is obtained only in the upper and central parts of the area of inversion. The estimated variations rapidly increase with the depth and to the sides of the inversion area, reaching almost 0.0001 S/m. The resolution density decreases for the bottom and edge parts of the inverse model, correspondingly, as shown in Figure 4.

This simple numerical example shows that, in the practical inversion of geophysical data, it is not enough to plot just the inverse model obtained by inversion. In principle, the data acquisition and inversion schemes, play rather important roles in the way the noise propagates into the inverse model. The newly developed method of model appraisal and resolution analysis makes it possible to locate the parts of inverse image that experience the minimal effect of the noise in the data and the areas with the strongest distortions. As a result, the interpreter can identify the parameters of the inverse model that can be treated with the most confidence, as well as less reliable features. This is the major practical significance of our method of inverse image appraisal.

RESOLUTION STUDY OF THE NONLINEAR 3D MAGNETOTELLURIC INVERSION ALGORITHM

In this section, we demonstrate the application of the developed method of the resolution analysis to a nonlinear, 3D MT inverse problem.

The foundations of the MT method were developed by Tikhonov (1950) and Cagniard (1953). It is based on measurements of the natural EM field at the surface of the earth. The interpretation of MT data is based on the calculation of the transfer functions between the horizontal components of the electric and magnetic fields, which form the so-called impedance tensor $\hat{\mathbf{Z}}$ (Berdichevsky and Dmitriev, 2002):

$$\hat{\mathbf{Z}} = \begin{bmatrix} Z_{xx} & Z_{xy} \\ Z_{yx} & Z_{yy} \end{bmatrix}. \tag{20}$$

The components of the impedance tensor are determined from the horizontal components of the electric and magnetic fields at each observation point. The corresponding technique for solving this problem is outlined in Zhdanov and Keller (1994) and Berdichevsky and Dmitriev (2002). These data are inverted for a conductivity model of the earth.

Thus, the MT inversion requires forward modeling of EM field components, the corresponding impedances, and the apparent resistivities and phases on each iteration step. This procedure is extremely time consuming, resulting in enormous calculations to solve the inverse problem. To overcome this computational difficulty, Zhdanov and Golubev (2003) suggest using an approximate solution based on quasi-analytic (QA) approximation on the initial stage of the iterative inversion. The detailed description of the basic principles of the QA approximation can be found in Zhdanov et al. (2000) and Zhdanov (2002). The approximate QA forward operators, introduced in the cited papers, can be used to compute the components of the impedance tensor $\hat{\mathbf{Z}}$. These operators significantly speed up the computations at each step of the inversion.

In a general case, the corresponding equations of MT inversion can be expressed by an operator equation including the data vector $\mathbf{d}$ and the vector of model parameters $\mathbf{m}$ as

$$\mathbf{d} = \mathbf{B}(\mathbf{m}), \tag{21}$$

where $\mathbf{B}$ is the nonlinear forward operator representing the governing equations of the MT impedance modeling problem, $\mathbf{m}$ is the vector of the unknown conductivity distribution (model parameters), and $\mathbf{d}$ is the vector formed by the observed values of the components of the MT impedance tensor at the observation points.

Inversion aims at estimating the model parameter vector $\mathbf{m}$ based on $\mathbf{B}$ and a known (observed) data vector $\mathbf{d}$. This problem is usually ill posed, i.e., the solution can be nonunique and unstable. The conventional way of solving ill-posed inverse problems, according to regularization theory (Tikhonov and Arsenin, 1977; Zhdanov, 2002), is based on minimization of the Tikhonov parametric functional, similar to one shown in equation 4.

To generate a focused image of the geoelectrical model, Zhdanov and Hursán (2000) and Mehanee and Zhdanov (2002) applied a minimum support stabilizer, which is a nonquadratic functional of a form

$$s_{MS}(\mathbf{m}) = (\mathbf{m} - \mathbf{m}_{\text{apr}})^T[(\hat{\mathbf{m}} - \hat{\mathbf{m}}_{\text{apr}})^2 + e^2\hat{\mathbf{I}}]^{-1}(\mathbf{m} - \mathbf{m}_{\text{apr}}), \tag{22}$$

where $\hat{\mathbf{m}}$ and $\hat{\mathbf{m}}_{\text{apr}}$ are $N_m \times N_m$ diagonal matrices of inverse-model parameters (current and a priori, respectively)

$$\hat{\mathbf{m}} = \mathbf{diag}(m_1, m_2, \ldots, m_{N_m}),$$

$$\hat{\mathbf{m}}_{\text{apr}} = \mathbf{diag}(m_{1\text{apr}}, m_{2\text{apr}}, \ldots, m_{N_m\text{apr}}),$$

where e is the focusing parameter and $\hat{\mathbf{I}}$ is an $N_m \times N_m$ identity matrix. Portniaguine and Zhdanov (1999) show that this functional minimizes an area of nonzero parameter distribution (minimizes the support of the inverse model) if e tends to zero: $e \to 0$. The principles of the minimum support inversion are discussed in detail in Zhdanov (2002).

Recently, Zhdanov and Tolstaya (2004) suggest using a nonlinear parameterization to transform the nonquadratic, minimum-support stabilizing functional described by equation 22 into a quadratic one, described by

$$\tilde{\mathbf{m}} = [(\hat{\mathbf{m}} - \hat{\mathbf{m}}_{\text{apr}})^2 + e^2\hat{\mathbf{I}}]^{-1/2}(\mathbf{m} - \mathbf{m}_{\text{apr}}), \tag{23}$$

and

$$\mathbf{m} - \mathbf{m}_{\text{apr}} = e[\hat{\mathbf{I}} - \hat{\tilde{\mathbf{m}}}^2]^{-1/2}\tilde{\mathbf{m}}, \tag{24}$$

where $\mathbf{m} = \{m_i\}$, $i = 1, \ldots, N_m$ is the original vector of the model parameters; $\tilde{\mathbf{m}} = \{\tilde{m}_i\}$, $i = 1, \ldots, N_m$ is a new vector of the nonlinear parameters; and $\hat{\tilde{\mathbf{m}}}$ is a $N_m \times N_m$ diagonal matrix with the diagonal formed by nonlinear model parameters, $\hat{\tilde{\mathbf{m}}} = \text{diag}(\tilde{m}_1, \tilde{m}_2, \ldots, \tilde{m}_{N_m})$.

We solve the minimization problem for the corresponding Tikhonov parametric functional by the regularized conjugate gradient (RCG) method. The details of this algorithm are described in Zhdanov and Tolstaya (2004).

The application of the QA approximation to forward modeling and Fréchet derivative computations speeds up the calculation dra-

matically. However, to control the accuracy of the inversion, this method allows application of rigorous forward modeling in the final steps of the inversion procedure. We use an integral equation forward-modeling code based on the contraction integral equation method, which improves the convergence rate of the iterative solvers (Hursán and Zhdanov, 2002). Application of a few additional iterations with a rigorous forward-modeling solver improves the resolution of the inverse method and helps to generate a more correct image of the target (Zhdanov and Tolstaya, 2004).

We now present a numerical example of the MT data inversion and the resolution analysis. Consider a homogeneous half-space with a resistivity of 100 ohm-m, containing a conductive dike. The resistivity of the inhomogeneity is 3 ohm-m. The top of the dike is at a depth of 200 m, and its bottom is at a depth of 600 m beneath the surface. This model is excited by a plane EM wave source. The x- and y-components of the anomalous magnetic and electric fields for four different frequencies (1, 10, 100, and 1000 Hz) have been simulated at 225 receiver points arranged on a homogeneous grid, using integral equation forward-modeling code INTEM3D (Hursán and Zhdanov, 2002). The coordinates of the receiver grid are x and y from -700 to 700 every 100 m. The receiver system is located at the surface of the earth. The EM field components were recalculated into MT impedances, using the standard equations (Berdichevsky and Dmitriev, 2002). The area of inversion is covered by a homogeneous mesh consisting of $16 \times 25 \times 8$ cubic cells surrounding the anomalous structure to be inverted. Each cell has a dimension of 100 m in the x-, y-, and z-directions. We select the focusing parameter as $e = 0.016$. The details of the technique for the optimum e selection can be found in Zhdanov and Tolstaya (2004).

Figure 5a shows the true model. For this model, we run inversion using different inverse methods. On the first stage, we ran 15 iterations of the RCG method with minimum norm stabilizer (Figure 5b); after that, we applied 60 iterations with a minimum-support stabilizer and QA forward modeling and an additional 20 iterations of the RCG method with minimum-support inversion and rigorous forward modeling (Figure 5c). The inversion curves, parametric functional $P[\alpha]$, stabilizer $s[\mathbf{m}]$, misfit $\phi[\mathbf{m}]$, and elapsed time versus iteration number are shown in Figure 5d, as well.

Figure 6 presents the vertical cross sections of the true model (panel a), the smooth inversion result with minimum-norm stabilizer (panel b), the intermediate result with minimum-support stabilizer and QA forward modeling (panel c), and the final focusing inversion result (panel d). One can see that the smooth minimum-norm result underestimates the true conductivity, while the focusing inversion reconstructs an image that is very close to the true model and with practically the same resistivity.

We have analyzed the resolution of our nonlinear-inversion method for the final model presented in Figure 5c and in Figure 6d. We computed the maximum possible variations in the solution of nonlinear-inverse problems for a conductive dike for a given level of relative errors in the observed data equal to 3%. The vertical sections of the upper bounds of the variations of conductivity distributions and the resolution density are shown in Figures 7 and 8. One can see that the resolution is higher in the central parts of the sections, and the

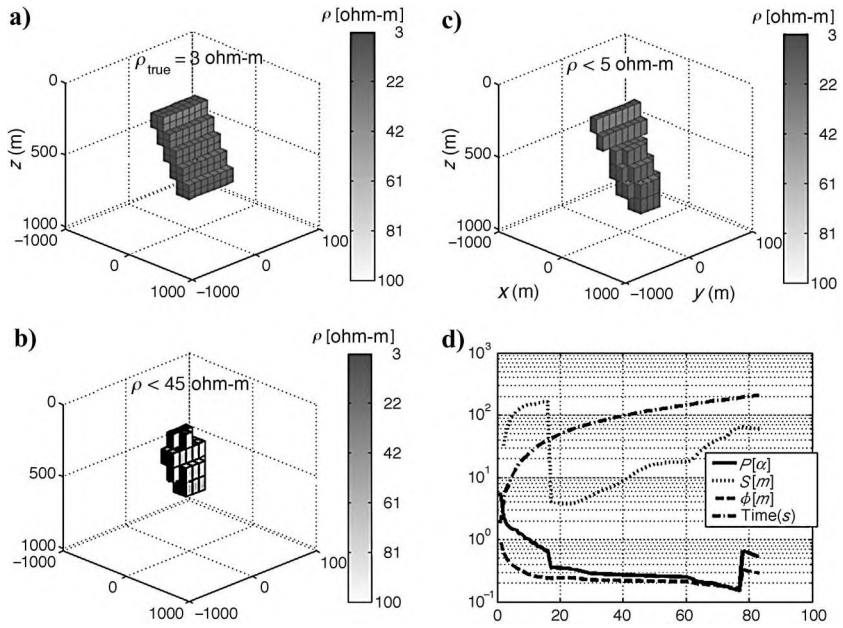

Figure 5. (a) The true model of a conductive dike. (b) Inversion results after 15 iterations with the minimum-norm stabilizer. (c) Final result after 60 iterations with the minimum-support stabilizer and QA forward modeling and 20 additional iterations of the RCG method with minimum-support inversion and rigorous full-forward modeling. (d) Inversion curves, parametric functional $P[\alpha]$, stabilizer $s[m]$, misfit $\phi[m]$, and elapsed time versus iteration number. In this figure, we present 3D images of the resistivity distribution with volume rendering. The cutoff level of the resistivity for these images is shown in the corresponding panels. For example, the cutoff level $\rho < 5$ ohm-m means that only the cells with a value of resistivity less than 5 ohm-m are displayed (after Zhdanov and Tolstaya, 2004).

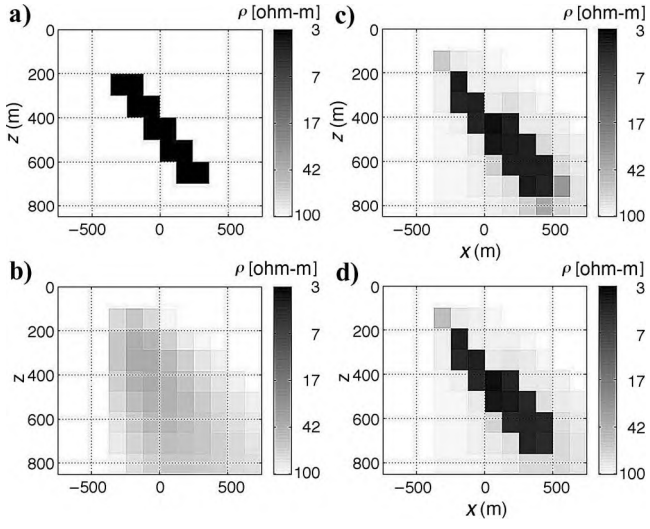

Figure 6. Dike model. Vertical cross sections of the true model (a), the inversion result with the minimum-norm stabilizer (b), the intermediate result with the minimum-support stabilizer and QA forward modeling (c), and the final sharp inversion result (d) (after Zhdanov and Tolstaya, 2004).

variations increase with the depth and to the sides of the inversion area. The maximum possible variations in the area of the dike location do not exceed 0.03 S/m, which constitutes less than 10% of the anomalous conductivity.

This example shows that by applying nonlinear regularized-focusing inversion, we obtain a very accurate image of the target. In this situation, the parameters of the true model are located within the upper bounds of the model parameter variations, provided by the resolution analysis.

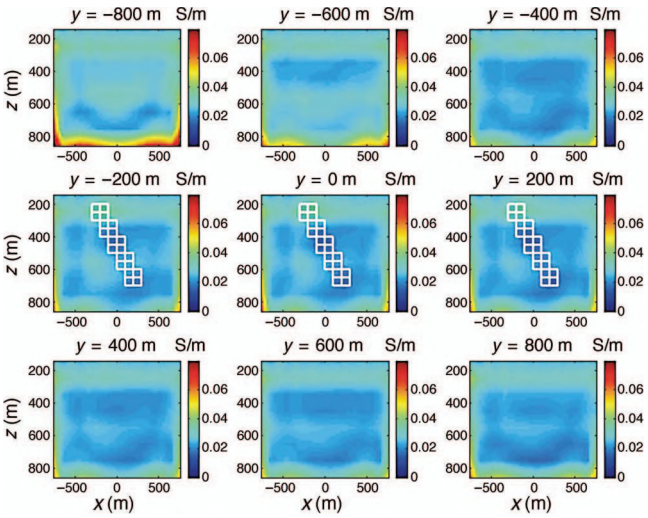

Figure 7. Model of the conductive dike. The vertical sections of the upper bounds of the conductivity variations $\delta\Delta\sigma_j(\mathbf{r})$ computed for the dike-model MT data inversion under the assumption that the relative error in the observed data is $\varepsilon = 3\%$. The white lines show the true position of the conductive dike.

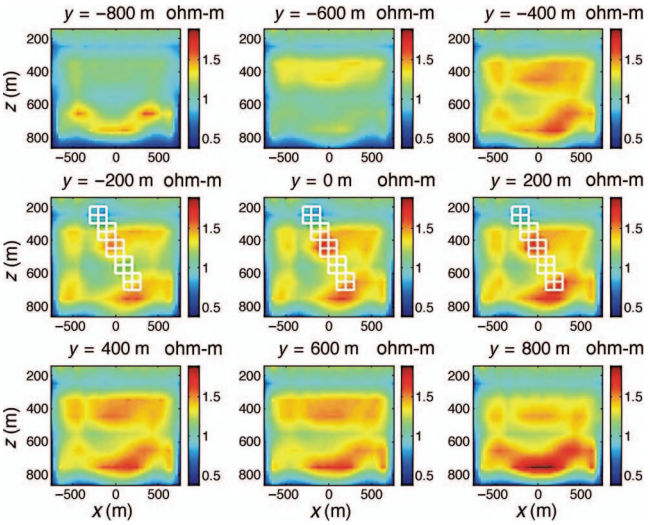

Figure 8. The vertical sections of the resolution density $R_{0l}^{\Delta\sigma r}$ distribution, computed for the model of the conductive dike. The white lines show the true position of the conductive dike.

CASE HISTORY: RESOLUTION STUDY OF 3D INVERSION OF HEM DATA COLLECTED IN THE VOISEY'S BAY AREA

We applied our method for the resolution analysis of the 3D inversion result to the real HEM data collected by INCO Exploration in the Voisey's Bay area in Canada to examine the resolution of the corresponding inverse model. This area is characterized by high-conductivity nickel-copper sulfide deposits hosted by resistive troctolite dikes (Naldrett et al., 1996). A geologic map of the area with several identified deposits is shown in Figure 9. Zhdanov and Tartaras (2002) used localized quasilinear inversion for the 3D interpretation of the HEM data collected within an area outlined in Figure 9. This area corresponds to the location of the Ovoid deposit, which is a flat-lying deposit of very high conductance comprised of 70% massive sulfide (Balch et al., 1998).

Here, we use the same data to demonstrate a new resolution-analysis technique. In the first stage, following Zhdanov and Chernyavskiy (2004), we apply an SLDM method for 3D inversion of the HEM data. Based on drilling information incorporated in Figure 9, we assume a 20-m deep, conductive overburden with resistivity of 10 ohm-m. We used the coplanar and coaxial components from the lowest frequency (900 Hz) because they are the least sensitive to the presence of the conductive overburden. The data were transformed from parts per million to anomalous field values in teslas, assuming a uniform background resistivity of 1900 ohm-m. The data comprise part of four flight lines at a distance of 200 m from each other (lines A, B, C, and D in Figure 9). The area of inversion was 700 m $\times$ 600 m $\times$ 160 m and was divided into $14 \times 30 \times 8$ cells.

Figure 10 presents the inversion result in the form of vertical slices through the model generated as a result of the inversion. Note that the vertical section at $x = 300$ m corresponds to flight line B, while the vertical section at $x = 500$ m corresponds to flight line C. Figure

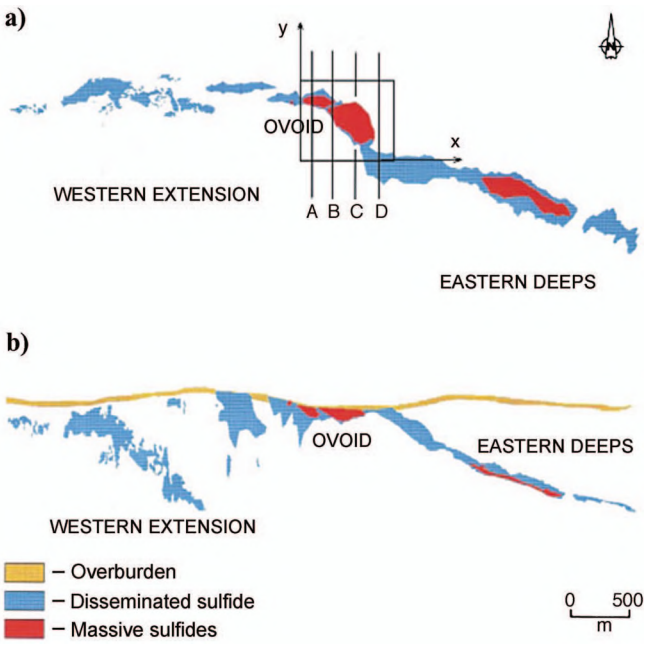

Figure 9. A map of the Voisey's Bay sulfide deposits. (a) Plan map. (b) North-facing longitudinal section. The data measured along four flight lines (A, B, C, and D) flown over the Ovoid deposit were used for inversion (after Zhdanov and Tartaras, 2002).

11 shows the observed and predicted data along flight line, A, B, C, and D, shown in Figure 9. The observed data are shown by solid lines. The predicted data obtained by full SLDM comprised of 200 Lanczos steps are shown by the dashed lines, while the dotted curves correspond to the truncated SLDM with only 25 Lanczos steps (Zhdanov and Chernyavskiy, 2004). One can see that the agreement between the three curves is very good. The results seem reasonable and in good agreement with the existing information about the Ovoid deposit (Balch et al., 1998) and with the inversion result obtained by Zhdanov and Tartaras (2002) using the LQL method with the conjugate gradient minimization.

We have evaluated the resolution of this inversion using a technique described in this paper. Figure 12 presents the vertical cross sections of the estimated variations of the conductivity $\delta\Delta\sigma_i(\mathbf{r})$ for the Voisey's Bay HEM data inversion. We can see in this figure that the estimated variations in the HEM data inversion in the area of the conductive target are within 0.03 S/m, while the maximum inverted conductivity of the Ovoid is about 1.5 S/m. We have assumed in these calculations that the relative error in the observed data is $\varepsilon = 1\%$. Thus, variations in the inversion do not exceed 2% within the volume of the conductive target. If we assume that the relative errors of the data could be as high as 10%, the maximum variations in the inverse model will be increased up to 30%, correspondingly. Figure 13 presents the resolution density $R_i^{\Delta\sigma}$ distribution for the same inverse model, shown in Figure 10. One can see that the resolution density decreases at the bottom and at the sides of the area of inversion. We observe the maximum resolution in the area of the conductive Ovoid deposit. The resolution density distribution and the plots of the upper bounds of the conductivity variations, $\delta\Delta\sigma_i(\mathbf{r})$, for the Voisey's Bay HEM data inversion provide a clear indication that the inversion result would not be distorted significantly by the noise in the data in the central area of the inversion domain, while the estimated variations increase with the depth and to the sides of the area of inversion.

We should note, however, that the true conductivity of the orebody in the area of investigation is much higher than 1.5 S/m obtained by the inversion. Therefore, in this case, the LQL inversion, as usual, underestimates the true conductivity, which is typical for a linearized smooth inversion, as in the case of our model study. At the same time, in airborne exploration for a mining target, similar to the HEM survey conducted in the Voisey's Bay area, it is very well known that the target has high conductivity. The problem is not to find the true conductivity of the mineralization zone but to correctly locate this target. In this situation, the LQL inversion provides a rea-

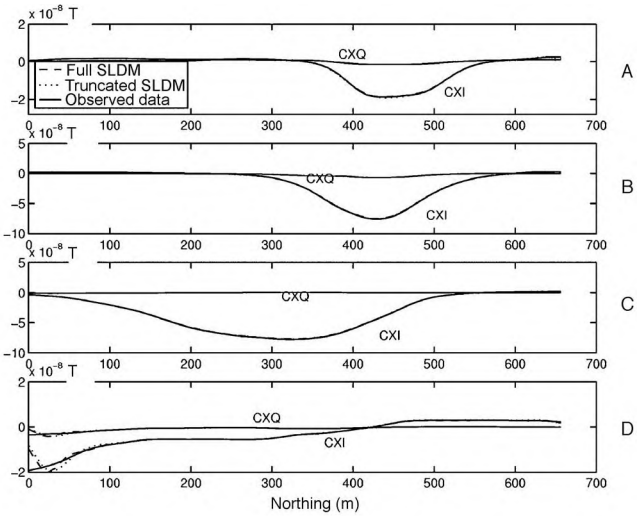

Figure 11. The magnetic field values along four south-north lines A, B, C, and D above the Ovoid. The observed field is shown along with the predicted fields for the inverse model obtained by the full and truncated SLDM method. The labels CXQ and CXI refer to the quadrature and in-phase components of the HEM data, respectively. The units for the vertical axis are teslas (T).

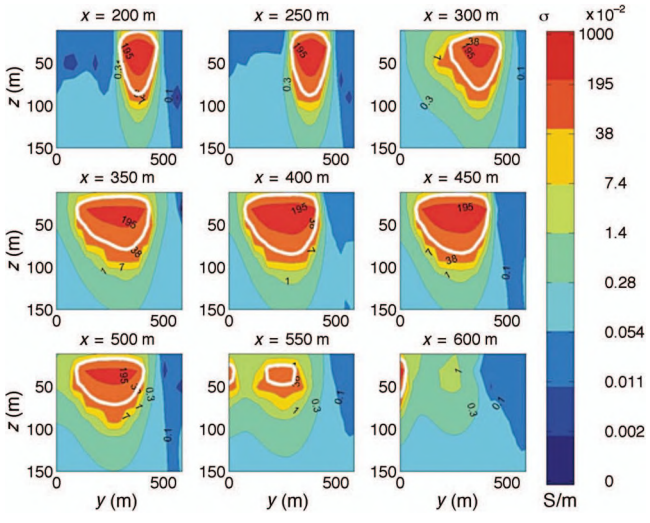

Figure 10. Vertical slices through the geoelectrical model generated as the result of the inversion for the Voisey's Bay HEM data. The vertical section at $x = 300$ m corresponds to flight line B; the section at $x = 500$ m corresponds to line C (Figure 9). The white outlines show the boundary of the conductive body with the conductivity more than 1 S/m, based on the inversion result.

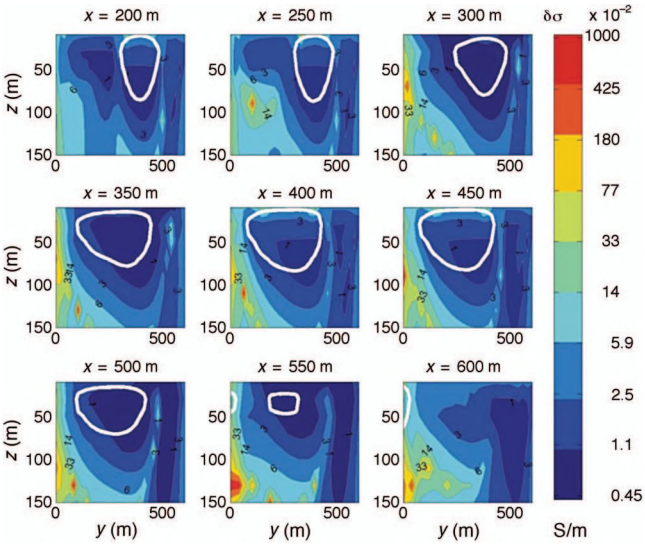

Figure 12. Vertical cross sections of the upper bounds of the conductivity variations $\delta\Delta\sigma_i(\mathbf{r})$ for the Voisey's Bay HEM data inversion. The white outlines show the boundary of the conductive body with the conductivity more than 1 S/m, estimated based on the inversion result.

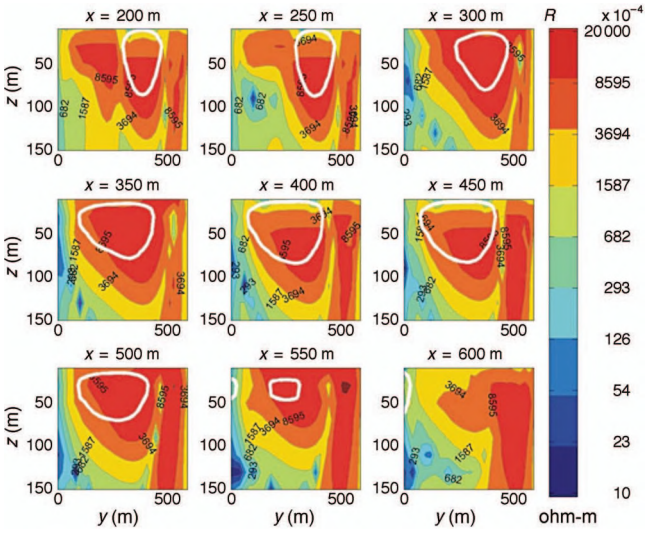

Figure 13. Vertical cross sections of the resolution density $R_i^{\Delta\sigma}$ distribution for the Voisey's Bay HEM data inversion. The white outlines show the boundary of the conductive body with the conductivity more than 1 S/m, estimated based on the inversion result.

sonable estimate of the location of the conductivity anomaly, while the resolution analysis confirms that this location would not change dramatically even if we consider the possible errors in the data and the inherent instability of the inverse problem. Therefore, we may conclude that we have a robust estimation of the location of the conductive body, even though the true conductivity is actually underestimated.

CONCLUSIONS

The existing techniques for appraisal of geophysical inverse images are based on calculating the data and model resolution and the covariance matrices. This technique provides, for example, a standard deviation of the model parameters from the inversion result. In many practical applications, however, it may be useful to also estimate the maximum possible variations in the solution of the inverse problem for the given errors in the observed data. These upper bounds of the model variations determine the actual resolution of geophysical inversion. We have developed a novel approach to the resolution analysis of the regularized geophysical inversion, based on evaluating the upper bounds of the model variations using the Cauchy inequality for the regularized least-squares solution of the linear inverse problem. The inverse of the upper bounds of the model parameter variations determines a new characteristic of geophysical inversion — a resolution density. We have also developed an efficient numerical method for the resolution density calculation based on the SLDM. This new technique provides a quantitative evaluation of the stability of the inverse problem solution by generating a spatial distribution of the upper bounds of the variations in the inverse model. At the same time, our method should be treated as a complement to the traditional methods of model appraisal and resolution analysis, which may provide additional insight in the inversion result.

This approach was extended to nonlinear inverse problems as well. Our extension is based on studying the sensitivity and resolution of the nonlinear inverse problem in the vicinity of the final solution. In this case, we approximate the relationship between the errors in the observed data and the corresponding variations in inversion results by the linear Fréchet derivative operator computed for the final solution. This approximation allows us to conduct the nonlinear resolution analysis based on the same principles that have been developed for the linear inverse problem.

The method is illustrated by the resolution analysis of linearized 3D HEM data inversion and nonlinear 3D MT inversion. In the case of linearized smoothed LQL inversion, we underestimate the true conductivity of the target while providing a stable estimate of its location. The full nonlinear 3D MT inversion with focusing regularization makes it possible to accurately recover both the conductivity and the shape and the location of the target. We should note, however, that the upper bounds of the model parameter variations may not represent the true errors of inversion (the errors which reflect the difference between the inverse model and the true model). The numerical examples show that the interpretation of these bounds depends on the method used for the inversion. If we apply the nonlinear regularized focusing inversion based on rigorous forward modeling, the upper bounds provide the correct errors of the inversion result. In the case of smooth inversion based on the approximate forward solutions (like the LQL inversion), the resolution density analysis provides useful information about the pattern of the noise transformation into the inverse image.

The important conclusion is that, using the new technique described in this paper, one can present the regularized inversion result in the form of both the model parameter and the estimated model variation distributions. Thus, the potential end user of the geophysical survey may analyze not only the inverse model produced by a specific inversion algorithm but also a spatial distribution of the upper bounds of the model parameter variations. This information may provide useful insight into the robustness of the inverse geophysical imaging.

The resolution study in the case history of the 3D HEM survey, shows that this new technique provides a useful tool for the analysis of the robustness of a geophysical inversion, which may complement the traditional methods of image appraisal. Although in this paper we present application examples in EM geophysical methods, it is possible to extend this theory to other geophysical methods as well.

ACKNOWLEDGMENTS

The authors acknowledge the support of the University of Utah Consortium for Electromagnetic Modeling and Inversion (CEMI), which includes BAE Systems, Baker Atlas Logging Services, BGP China National Petroleum Corporation, BHP Billiton World Exploration Inc., Centre for Integrated Petroleum Research, EMGS, ENI, ExxonMobil Upstream Research Company, INCO Exploration, Information Systems Laboratories, MTEM, Newmont Mining Co., Norsk Hydro, OHM, Petrobras, Rio Tinto-Kennecott, Rocksource, Schlumberger, Shell International Exploration and Production Inc., Statoil, Sumitomo Metal Mining Co., and Zonge Engineering and Research Organization.

We also thank INCO Exploration, and particularly A. King, for providing us with the HEM data set.

The authors are grateful to the anonymous reviewers for their comments and recommendations, which improved the paper.

APPENDIX A

APPLICATION OF THE SPECTRAL LANCZOS DECOMPOSITION METHOD (SLDM) FOR RESOLUTION DENSITY CALCULATION

In this appendix, we construct a numerical algorithm for resolution-density calculation.

According to the definition, the resolution density is obtained by adding the squares of the column elements of the regularized inverse matrix $\mathbf{R}_\alpha$. To find the ith column of this matrix, we can introduce a vector $\mathbf{e}_i$ with unity in the ith position:

$$\mathbf{e}_i = [0,0, \ldots, 0,1,0, \ldots, 0]^T \in E^{N_d},$$

where E^{N_d} is N_d-dimensional Euclidean space, and recover the ith column of the regularized inverse matrix $\mathbf{R}_\alpha^{(i)}$ by simple multiplication:

$$\begin{aligned}\mathbf{R}_\alpha^{(i)} &= (\mathbf{A}^*\mathbf{W}_d^2\mathbf{A} + \alpha\mathbf{W}_m^2)^{-1}\mathbf{A}^*\mathbf{W}_d^2\,\mathbf{e}_i \\ &= \mathbf{W}_m^{-2}(\mathbf{A}^*\mathbf{W}_d^2\mathbf{A}\,W_m^{-2} + \alpha\mathbf{I})^{-1}\mathbf{A}^*\mathbf{W}_d^2\,\mathbf{e}_i. \qquad \text{(A-1)}\end{aligned}$$

Introducing the notations

$$\mathbf{B} = \mathbf{A}^*\mathbf{W}_d^2\mathbf{A}\mathbf{W}_\mathbf{m}^{-2}, \quad \mathbf{c}_i = \mathbf{A}^*\mathbf{W}_d^2\,\mathbf{e}_i,$$

we finally obtain

$$\mathbf{R}_\alpha^{(i)} = \mathbf{W}_m^{-2} f_\alpha(\mathbf{B})\mathbf{c}_i, \qquad \text{(A-2)}$$

where

$$f_\alpha(\mathbf{B}) = (\mathbf{B} + \alpha\mathbf{I})^{-1}.$$

Thus, we have arrived at the problem of computing a function of matrix $\mathbf{B}$.

This problem can be solved by the SLDM (Druskin and Knizhnerman, 1994; Golub and Van Loan, 1996; Zhdanov, 2002). First, we apply the Lanczos algorithm for QT decomposition of matrix $\mathbf{B}$:

$$\beta_0 = 1, \quad \mathbf{q}_0 = 0, \quad \mathbf{q}_1 = \mathbf{c}_i, \qquad \text{(A-3a)}$$

$$\text{while } \beta_j \neq 0, \quad \mathbf{q}_{j+1} = \frac{\mathbf{r}_j}{\beta_j}, \quad \alpha_j = \mathbf{q}_j^*\mathbf{B}q_j, \qquad \text{(A-3b)}$$

$$\mathbf{r}_j = (\mathbf{B} - \mathbf{I}_\mathbf{N})\mathbf{q}_j - \beta_{j-1}\mathbf{q}_{j-1}, \quad \beta_j = \|\mathbf{r}_j\|, \qquad \text{(A-3c)}$$

$$j = 1, 2, \ldots, N-1.$$

As a result, we find an orthogonal matrix $\mathbf{Q}_L$ and the tridiagonal matrix $\mathbf{T}_L$, where L is an iteration step of the Lanczos algorithm.

We can write expression A-2 as

$$\mathbf{R}_\alpha^{(i)} = \mathbf{W}_m^{-2}\|\mathbf{c}_i\|\mathbf{Q}_L f_\alpha(\mathbf{T}_L)\mathbf{e}_1^{(L)} = \mathbf{W}_m^{-2}\|\mathbf{c}_i\|\mathbf{Q}_L(\mathbf{T}_L + \alpha\mathbf{I})^{-1}\mathbf{e}_1^{(L)}, \qquad \text{(A-4)}$$

where

$$\mathbf{e}_1^{(L)} = [1,0, \ldots, 0,0, \ldots, 0]^T \in E^L.$$

The resolution density is computed now, according to equation 9, as

$$\mathcal{R}_i = \|\mathbf{d}\|^{-1}\left[\sum_{j=1}^{N_d} |R_{\alpha ij}|^2\right]^{-1/2}. \qquad \text{(A-5)}$$

The advantage of the SLDM method is that we have to run the Lanczos algorithm only once for all different values of the regularization parameter α. After that we only have to invert a tridiagonal matrix $(\mathbf{T}_L + \alpha\mathbf{I})$ for a different α, which is a much simpler operation.

The selection of the optimal regularization parameter α can be made using either Tikhonov's method or the L-curve method. The detailed description of these methods can be found in Zhdanov (2002).

REFERENCES

Alumbaugh, D. L., and G. N. Newman, 2000, Image appraisal for 2D and 3D electromagnetic inversion: Geophysics, **65**, 1455–1467.

Backus, G. E., 1970a, Inference from inadequate and inaccurate data, I: Proceedings of the National Academy of Sciences, **65**, 1–7.

———, 1970b, Inference from inadequate and inaccurate data, II: Proceedings of the National Academy of Sciences, **65**, 281–287.

———, 1970c, Inference from inadequate and inaccurate data, III: Proceedings of the National Academy of Sciences, **67**, 282–289.

Backus, G. E., and T. I. Gilbert, 1967, Numerical applications of a formalism for geophysical inverse problems: Geophysical Journal of the Royal Astronomical Society, **13**, 247–276.

———, 1968, The resolving power of gross earth data: Geophysical Journal of the Royal Astronomical Society, **16**, 169–205.

Balch, S. J., T. J. Crebs, A. King, and M. Verbiski, 1998, Geophysics of the Voisey's Bay Ni-Cu-Co deposits: 68th Annual International Meeting, SEG, Expanded Abstracts, 784–787.

Berdichevsky, M. N., and V. I. Dmitriev, 2002, Magnetotellurics in the context of the theory of ill-posed problems: SEG.

Cagniard, L., 1953, Theory of magnetotelluric method of geophysical prospecting: Geophysics, **18**, 605–635.

Dmitriev, V. I., M. S. Zhdanov, V. A. Morozov, A. A. Nikitin, and H. P. Brusnetsov, eds., 1990, Computational mathematics and techniques in exploration geophysics (in Russian): Nedra Press.

Druskin, V., and L. Knizhnerman, 1994, Spectral approach to solving three-dimensional Maxwell's diffusion equations in the time and frequency domains: Radio Science, **29**, 937–953.

Druskin, V., L. Knizhnerman, and P. Lee, 1999, New spectral Lanczos decomposition method for induction modeling in arbitrary 3D geometry: Geophysics, **64**, 701–706.

Foster, M., 1961, An application of the Wiener-Kolmogorov smoothing theory to matrix inversion: Journal of the Society for Industrial and Applied Mathematics, **9**, 387–392.

Franklin, J. N., 1970, Well-posed stochastic extensions of ill-posed linear problems: Journal of Mathematical Analysis and Applications, **31**, 682–716.

Golub, G. H., and C. F. Van Loan, 1996, Matrix computations, 3rd ed.: Johns Hopkins Univ. Press.

Hursán, G., and M. S. Zhdanov, 2002, Contraction integral equation method in 3D electromagnetic modeling: Radio Science, **37**, 1089 doi:10.1029/2001RS002513.

Jackson, D. D., 1972, Interpretation of inaccurate, insufficient and inconsistent data: Geophysical Journal of the Royal Astronomical Society, **28**, 97–110.

Lanczos, C., 1961, Linear differential operators: D. van Nostrand Co.

Marquardt, D. W., 1963, An algorithm for least-squares estimation of nonlinear parameters: Journal of the Society for Industrial and Applied Mathematics, **11**, 431–441.

———, 1970, Generalized inverses, ridge regression, biased linear estimation, and nonlinear estimation: Technometrics, **12**, 591–612.

McGillivray, P. R., and D. W. Oldenburg, 1990, Methods for calculating Fréchet derivatives and sensitivities for the nonlinear inverse problem: A comparative study: Geophysical Prospecting, **38**, 499–524.

McGillivray, P. R., D. W. Oldenburg, R. G. Ellis, and T. M. Habashy, 1994, Calculation of sensitivities for the frequency-domain electromagnetic problem: Geophysical Journal International, **116**, 1–4.

Mehanee, S., and M. S. Zhdanov, 2002, Two-dimensional magnetotelluric inversion of blocky geoelectrical structures: Journal of Geophysical Research, **107**, B4, 2065, doi:10.1029/2001JB000191.

Menke, W., 1989, Geophysical data analysis: Discrete inverse theory: Academic Press Inc.

Naldrett, A. J., H. Keats, K. Sparkes, and S. Moore, 1996, Geology of the Voisey's Bay Ni-Cu-Co deposit, Labrador, Canada: Exploration and Mining Geology, **5**, 169–179.

Oldenburg, D. W., 1983, Funnel functions in linear and nonlinear appraisal: Journal of Geophysical Research, **88**, B9 7387–7398.

Parker, R. L., 1975, The theory of ideal bodies for gravity interpretation: Geophysical Journal of the Royal Astronomical Society, **42**, 315–334.
Portniaguine, O., and M. S. Zhdanov, 1999, Focusing geophysical inversion images: Geophysics, **64**, 874–887.
Ramirez, A. L., W. D. Daily, and R. L. Newmark, 1995, Electrical resistance tomography for steam injection monitoring and control: Journal of Environmental and Engineering Geophysics, **0**, 39–52.
Rodi, W. L., 1976, A technique for improving the accuracy of finite element solutions for magnetotelluric data: Geophysical Journal of the Royal Astronomical Society, **44**, 483–506.
Sabatier, P. C., 1977a, On geophysical inverse problems and constraints: Journal of Geophysical Research, **43**, 115–137.
———, 1977b, Positivity constraints in linear inverse problems — I. General theory: Geophysical Journal of the Royal Astronomical Society, **48**, 415–441.
———, 1977c, Positivity constraints in linear inverse problems — II. Applications: Geophysical Journal of the Royal Astronomical Society, **48**, 443–459.
Sambridge, M., and K. Mosegaard, 2002, Monte Carlo methods in geophysical inverse problems: Reviews of Geophysics, **40**, 3, 1–29.
Spies, B. R., and T. M. Habashy, 1995, Sensitivity analysis of cross-well electromagnetics: Geophysics, **60**, 834–845.
Stark, P. B., and R. L. Parker, 1987, Velocity bounds from statistical estimates of $t(p)$ and $X(p)$: Journal of Geophysical Research, **92**, B3, 2713–2719.
Stark, P. B., R. L. Parker, G. Masters, and L. A. Orcutt, 1986, Strict bounds on seismic velocity in the spherical earth: Journal of Geophysical Research, **91**, B14, 13892–13902.
Tarantola, A., 1987, Inverse problem theory: Elsevier Science Publ. Co. Inc..
Tarantola, A., and B. Valette, 1982, Generalized nonlinear inverse problem solved using the least squares criterion: Reviews of Geophysics and Space Physics, **20**, 219–232.
Tikhonov, A. N., 1950, On determining electric characteristics of the deep layers of the earth's crust: Doklady Akademii Nauk SSSR, **73**, 295–297.
Tikhonov, A. N., and V. Y. Arsenin, 1977, Solution of ill-posed problems: W. H. Winston and Sons.
Xiong, Z., 1992, EM modeling of three-dimensional structures by the method of system iteration using integral equations: Geophysics, **57**, 1556–1561.
Zhdanov, M. S., 2002, Geophysical inverse theory and regularization problems: Elsevier Science Publ. Co., Inc.
Zhdanov, M. S., and A. Chernyavskiy, 2004, Rapid three-dimensional inversion of multi-transmitter electromagnetic data using the spectral Lanczos decomposition method: Inverse Problems, **20**, S233–S256.
Zhdanov, M. S., V. I. Dmitriev, S. Fang, and G. Hursán, 2000, Quasi-analytical approximations and series in electromagnetic modeling: Geophysics, **65**, 1746–1757.
Zhdanov, M. S., and N. G. Golubev, 2003, Three-dimensional inversion of magnetotelluric data in complex geological structures, *in* J. Macnae and G. Liu, eds., Three-dimensional electromagnetics III, Australian Society of Exploration Geophysics.
Zhdanov, M. S., and G. Hursán, 2000, 3D electromagnetic inversion based on quasi-analytical approximation: Inverse Problems, **16**, 1297–1322.
Zhdanov, M. S., and G. W. Keller, 1994, The geoelectrical methods in geophysical exploration: Elsevier Science Publ. Co., Inc..
Zhdanov, M. S., and E. Tartaras, 2002, Inversion of multi-transmitter 3D electromagnetic data based on the localized quasi-linear approximation: Geophysical Journal International, **148**, 506–519.
Zhdanov, M. S., and E. Tolstaya, 2004, Minimum support nonlinear parameterization in the solution of 3D magnetotelluric inverse problem: Inverse Problems, **20**, 937–952.